PAPER

Check for updates

Comparative analysis of the properties of colorless and transparent polyimide nanocomposites with and without fluorine substitution

Moon Young Choi,[a] Ae Ran Lim [ID] *[ab] and Jin-Hae Chang [ID] *[c]

Two types of polyamic acids (PAAs) were synthesized using 4-(2,5-dioxotetrahydrofuran-3-yl)-1,2,3,4-tetrahydro-naphthalene-1,2-dicarboxylic anhydride and two diamines, 2,2-bis[4-(4-aminophenoxy) phenyl] propane and 2,2-bis[4-(4-aminophenoxy)phenyl]hexafluoropropane. Colorless and transparent polyimide (CPI) hybrid films were synthesized by dispersing various amounts (1−4 wt%) of Cloisite 30B (CS30B) into a PAA matrix using a solution intercalation method. The thermomechanical properties, clay dispersion morphology, optical transparency, and solubility of the two types of CPI hybrid films synthesized using different monomer structures were evaluated at various CS30B concentrations, and the results were compared. An increase in the thermomechanical properties of the CPI hybrid films was observed with only a small amount of organoclay dispersion, and the maximum enhancement in the physical properties occurred at a specific, critical clay content. Electron microscopy revealed that at low concentrations, the clay was uniformly dispersed throughout the polymer matrix at the nanoscale level but aggregated when added beyond a critical level. Structural changes in the CPI monomers and variations in CS30B content significantly influenced the physical properties of the CPI hybrid films. This study also highlighted the structure of an eco-friendly CPI designed to exhibit desirable physical properties without halogen elements, such as fluorine, which are environmentally regulated substances.

1. Introduction

Polyimide (PI) is a super engineering plastic with a main chain containing an imide ring and an amorphous structure. Aromatic PI exhibits outstanding heat resistance, chemical resistance, dimensional stability, and excellent electrical and mechanical properties. These advantages arise from its rigid chain structure of imide aromatic compounds and the interaction of its π electron charges.[1–3] Owing to these properties, PI is applicable in various fields such as automotive, aerospace, electrical, electronics, and solar cells. Furthermore, their lightweight, flexible nature allows their broad use in creating lighter, smaller products.[4,5]

Various studies have been conducted on materials suitable for transparent, flexible display devices. Historically, indium tin oxide (ITO) glass substrates have been commonly used in display devices.[6,7] However, ITO glass is fragile, heavy, and bulky, and its incompatibility with roll-to-roll processing renders its mass production unfeasible. In contrast, plastic materials such as PI are lighter and more flexible than ITO and can be mass-produced through roll-to-roll processes. Also, thermal stability is crucial because display substrates must withstand high temperatures during manufacturing. Therefore, PI, known for its outstanding heat resistance, is an ideal choice. However, conventional PI has been limited in its application to transparent displays owing to its low processability, which results from its insolubility, infusibility, and inherent brown color.[8–10]

The brown color of the PI can be attributed to the charge transfer complex (CTC) effect, which occurs during the formation of intra- and/or intermolecular CTCs within the polymer chain. Various methods have been employed to mitigate the CTC effect and enhance the optical transparency of PI. For instance, the linearity of the polymer chain structure has been reduced by using *meta* (*m*)-substituted monomers, and the mobility of π electrons in the PI chain has been suppressed by introducing strongly electron-withdrawing groups such as trifluoromethyl (–CF$_3$) or sulfone (–SO$_2$–) groups.[11–13] Recently, many efforts have been made to increase the optical transparency of PIs by employing alicyclic ring structures in dianhydride monomers.[14,15] These methods improve the colorless transparency of PI films by limiting the movement of π electrons and disrupting covalent bonding between molecules, minimizing the occurrence of CTC.

aGraduate School of Carbon Convergence Engineering, Jeonju University, Jeonju 55069, Korea

bDepartment of Science Education, Jeonju University, Jeonju 55069, Korea. E-mail: arlim@jj.ac.kr

cInstitute of Carbon Technology, Jeonju University, Jeonju 55069, Korea. E-mail: jhchang@jj.ac.kr

Numerous researchers have recently synthesized colorless, transparent polyimides (CPI) using a series of low-cost, synthetically developed alicyclic dianhydride-substituted tetralin (tetrahydro-naphthalene)-containing monomers.[16] The substituents on tetralin dianhydride included alkyl, fluorine, and chloromethyl groups. The CPIs synthesized using these substituents display diverse functionalities. These dianhydrides achieve high yield and purity upon polymerization and can be mass-produced at low cost. Kilogram-scale synthesis is feasible even in laboratory settings. Consequently, PI-containing alicyclic dianhydride monomers have garnered significant interest because of their potential use in the fabrication of liquid crystal display substrates, flexible solar cell substrates, organic electroluminescent panels, light guide plates, and materials with low dielectric constants.[17,18] 4-(2,5-Dioxotetrahydro furan-3-yl)-1,2,3,4-tetrahydro-naphthalene-1,2-dicarboxylic anhydride (DTDA), a type of tetralin dianhydride, has been extensively used in the development of high-performance, highly soluble PI, orientation layers for liquid crystals, layer alignment in PIs, and ultrafiltration membranes. Some time ago, Matsumoto et al.[19,20] synthesized a highly soluble CPI using DTDA and its derivatives as representative dianhydride monomers. The asymmetrical tetralin dianhydride structure in DTDA increases the reactivity of the monomer, resulting in a CPI characterized by excellent solubility and optical transparency.

Organic/inorganic composite materials maximize the interfacial adhesion of nanometer-sized composite materials, resulting in superior thermal and mechanical properties compared to conventional composite materials.[21,22] In particular, polymer/clay nanocomposite materials offer superior physical properties even with a smaller amount of clay than commonly produced microscale polymer composites. Moreover, the extent to which clay was dispersed and exfoliated significantly affected the physical properties of the nanocomposites.

When nanosized fillers are uniformly dispersed within the polymer matrix at the nanoscale, the thermomechanical properties of the polymer hybrid are improved, and the dimensional stability also increases.[23] Common nanofillers include clays, carbon nanotubes (CNTs), and graphene.[24,25] However, because most nanofillers exhibit low dispersibility or miscibility within the matrix, they may compromise the physical properties of hybrid materials. This issue can be addressed using organoclays, organo-CNTs, or functionalized graphene obtained through organic modification of molecules on the surface of the filler.[26] The synthesized organic filler enhanced dispersibility and compatibility by increasing reactivity with organic polymers. This allows for a uniform dispersion at the nanoscale within the polymer matrix without phase separation, ultimately enabling the production of nanoscale hybrid composites.

Commonly used types of clay include montmorillonite (MMT), bentonite, saponite, hectorite, and mica. MMT belongs to the smectite series and has a silicate layer structure. Due to its excellent dispersion and absorption and unique catalytic characteristics, MMT has found applications in various fields, such as dehumidifiers, medicines, cosmetics, and fillers; it is particularly effective as a nanofiller in hybrid materials. MMT is frequently used in various Cloisite organoclay series, wherein the clay surface is chemically treated with alkyl groups. This treatment enhances the distribution and compatibility of organic-inorganic hybrids.[27,28]

Most CPIs have utilized fluorine-containing monomers to reduce CTCs and achieve colorless transparency. However, halogen elements, including fluorine, are environmentally regulated and considered toxic, making them unsuitable for materials that prioritize eco-friendliness. Consequently, our ongoing research is focused on the synthesis of halogen-free CPIs. This study aimed to explore the potential of an eco-friendly CPI by comparing its physical properties with and without fluorine.

In this study, two new types of CPIs were synthesized by reacting the alicyclic dianhydride DTDA with the diamines 2,2-bis[4-(4-aminophenoxy)phenyl]propane (BAPP) and 2,2-bis[4-(4-aminophen-oxy)phenyl]hexafluoropropane (6FBAPP). We investigated the effect of the monomers BAPP and 6FBAPP, which have the same structure but differ in the presence of hydrogen (H) or fluorine (F), on CPI films obtained by reaction with DTDA. DTDA contains an alicyclic ring with a bent structure, which not only inhibits CTC but also helps maintain its colorless and transparent properties.

The main objectives of this study were to synthesize new CPIs using two different monomers with various substituents and to evaluate the thermomechanical properties, clay dispersion state, and optical transparency of CPI hybrid films based on varying concents of dispersed Cloisite 30B (CS30B; 1–4 wt%).
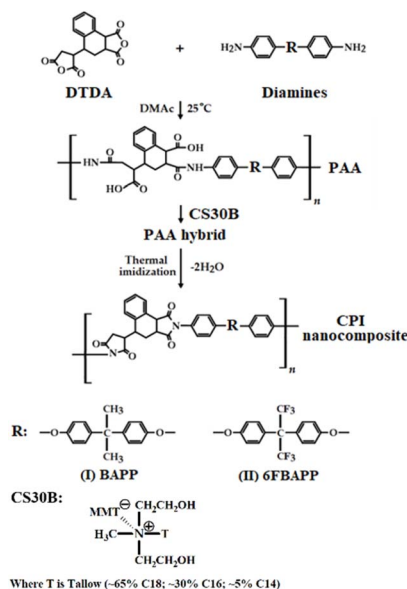
2. Experimental

2.1. Materials

The dianhydride DTDA and diamines BAPP and 6FBAPP, utilized in the CPI syntheses for this experiment, were procured from TCI (Tokyo, Japan). The solvent N,N'-dimethylacetamide (DMAc) was obtained from Junsei Chemical Co., Ltd. (Tokyo, Japan) and thoroughly dried over 4 Å molecular sieves before use. Organoclay CS30B was sourced from Southern Clay (Gonzales, TX, USA); its cation exchange capacity of MMT was measured at 90 meq./100 g.[29]

CS30B, an organophilic clay, possesses various types of alkyl groups, including very long alkyl chains, substituted on the clay surface, which impart strong organophilic properties.[30] This organophilicity provides excellent dispersibility and compatibility with the organic polymer matrix (CPI), enabling the formation of nanocomposites. The structure of CS30B is shown in Scheme 1. The long alkyl chains in CS30B widen the interlayer spacing (gallery) of the clay, facilitating the insertion of polymer chains between the clay layers.

2.2. Synthesis of PAA and CPI hybrid films

Despite variations in the diamine type, the experimental methods for the two CPI series were identical. For instance, in the synthesis of a CS30B 1 wt% hybrid film using diamine BAPP : DTDA (3.00 g, 1.0×10^{-2} mol) was dissolved in 3.5 mL of DMAc in a 100 mL three-necked flask and stirred at 25 °C for

Scheme 1 Synthetic route for CPIs based on (I) BAPP and (II) 6FBAPP diamine monomers.

Table 1 Heat-treatment conditions of CPI hybrid films

Sample	Temp., °C/time, h/pressure, Torr
PAA	$25/14/760 \rightarrow 50/1/1 \rightarrow 80/1/1$
CPI hybrid	$110/0.5/1 \rightarrow 140/0.5/1 \rightarrow 170/0.5/1 \rightarrow 195/1/1 \rightarrow 220/1/1 \rightarrow 235/2/1$

30 min. BAPP (5.18 g, 1.0×10^{-2} mol) was dissolved in 3.5 mL of DMAc in a separate flask. The BAPP and DTDA solutions were mixed and reacted vigorously at 25 °C for 14 h to obtain the PAA solution. CS30B (0.07 g) was dispersed in 3 mL of DMAc for 4 h. The dispersion was then combined with the PAA solution and stirred at 25 °C for 30 min. The resulting mixture was poured onto a 10×10 cm glass plate and heat-treated under vacuum to produce a hybrid film. The monomer structure and synthesis process of CPI are shown in Scheme 1.

The PAA solution solvent was removed by vacuum heating at 50 and 80 °C for 1 h each. Several heat treatment stages from 110 to 235 °C completed the CPI hybrid film synthesis. To ensure consistent 235 °C completed the CPI hybrid film synthesis. To ensure consistent physical properties, a constant thickness within the 43–46 μm range was maintained for all CPI hybrid films. The detailed heat-treatment conditions for the hybrid-film syntheses are summarized in Table 1.

2.3.   Characterization

Fourier-transform infrared spectroscopy (FT-IR; PerkinElmer, Spectrum Two, Llantrisant, UK) was used to verify the structure of the synthesized CPI film. To obtain more detailed information from the FT-IR data, solid-state ^{13}C cross-polar/magic angle rotation nuclear magnetic resonance spectroscopy (CP/MAS NMR; JEOL, JNM-ECZ400R/S3, Tokyo, Japan) was used to confirm the peak chemical shifts. The Larmor frequency (ω_0) of NMR was 100.52 MHz, based on the signal of tetramethylsilane (TMS). The three-dimensional (3D) structure of the polymer chains was analyzed using ChemDraw Office.

The dispersion states and interlayer distances of the nano-fillers in the matrix were investigated using wide-angle X-ray diffraction (XRD; Malvern Panalytical X'Pert, Amsterdam, Netherlands). Cu-Kα was employed as the target, the measurement range set to $2\theta = 2–12°$, and the measurement speed adjusted to 2° per min. To complement the XRD data, a transmitting electron microscope (TEM; FEI, Titan G2 Cube 60-300, Oregon, USA) was used to confirm the dispersion state and morphology of the clay layers in more detail. The specimens were prepared using cryogenic-focused ion beam scanning electron microscopy (FEI, Oregon, USA).

To investigate the thermal properties of the hybrid CPI films, differential scanning calorimetry (DSC; NETZSCH 200F3, Berlin, Germany) and thermogravimetric analysis (TGA; TA Instruments Q-500, New Castle, DE, USA) were employed. The experimental conditions were set at 10 °C min^{-1} under a nitrogen atmosphere. The coefficient of thermal expansion (CTE) was measured using a thermomechanical analyzer (TMA; TA Instruments TMA 2940, Tokyo, Japan) with a load of 0.1 N and a heating rate of 5 °C min^{-1}.

Mechanical tensile properties were measured using a universal testing machine (UTM; Shimadzu, JP/AG-50KNX, Tokyo, Japan). The sample size was 5 mm $\times$ 50 mm, and the crosshead speed was 5 mm min^{-1}. The results were obtained by measuring each sample more than ten times, and values outside the error range were excluded. The remaining results were averaged.

For optical properties, the optical transmittance and cutoff wavelength (λ_0) were measured using an ultraviolet-visible spectrometer (UV-Vis; Shimadzu UV-3600, Tokyo, Japan). The yellowness index (YI) was measured using a spectrophotometer (KONICA MINOLTA, CM-3600d, Tokyo, Japan).

3.   Results and discussion

3.1.   FT-IR and solid-state ^{13}C-NMR

The structure and synthesis of CPI were determined from the characteristic FT-IR peaks shown in Fig. 1. In the case of CPI using BAPP as the diamine in Fig. 1(I), the stretching peaks of the main-chain carbonyl group C=O appeared at 1780 cm^{-1} and 1706 cm^{-1}, respectively, and the C=C stretching peak was observed at 1502 cm^{-1}. Successful imidization was confirmed by the appearance of the imide group C–N–C peak at 1380 cm^{-1}.[31] For diamine 6FBAPP, as shown in Fig. 1(II), similar to BAPP, carbonyl group stretching peaks were confirmed at 1780 cm^{-1} and 1706 cm^{-1}, with a C=C peak at 1498 cm^{-1}. CPI synthesis was finally confirmed by observing the C–N–C peak at 1382 cm^{-1}.

Solid-state ^{13}C NMR spectroscopy provided more detailed confirmation of the CPI structure,[32] initially verified by FT-IR spectroscopy. Upon analysis of the ^{13}C-NMR spectrum of structure I, peaks corresponding to alicyclic carbons (a, d, and e) appeared at 24.69, 41.32, and 45.69 ppm; peaks corresponding
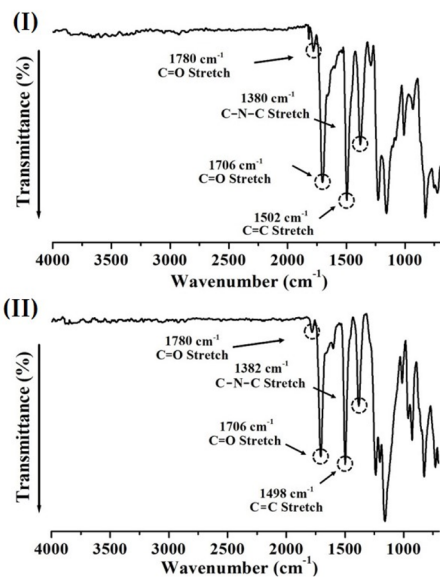
Fig. 1 FT-IR spectra of PAA and CPI.

Fig. 2 ^{13}C-NMR spectra of CPIs based on (I) BAPP and (II) 6FBAPP diamine monomers.

to carbons in benzene (f–k) were observed at 124.62, 131.42, 149.47, and 159.75 ppm. The methyl carbon (b) and the central carbon (c) of the isopropylene moiety were observed at 34.97 and 41.32 ppm, respectively, whereas the carbon (l) in the imide structure was observed at 179.68 ppm.

Structure II, which contains the strongly electron-withdrawing –CF$_3$ substituent, exhibited different chemical shifts than Structure I. Peaks corresponding to cycloaliphatic carbons (a–c) appeared at 24.24, 40.87, and 43.28 ppm; peaks corresponding to benzene carbons (f–k) were observed at 125.69, 132.04, 159.75, and 161.72 ppm, respectively. The central carbon (d) of the isopropylene structure was observed at 67.68 ppm and the –CF$_3$ carbon (e) at 125.69 ppm. The carbon atom (l) of the imide structure was observed at 179.77 ppm. In Fig. 2(I) and (II), the spinning sidebands of phenol are marked with asterisks (*).[32] The chemical shifts depicted in Fig. 2 correspond well with the chemical structure of the synthesized CPI, confirming the successful synthesis using NMR and FT-IR.

3.2. 3D polymer structures through computer simulation

Fig. 3 shows the 3D chemical structures of the two CPI films. In this structure, green, white, and red represent carbon, hydrogen, and fluorine atoms, respectively. The fluorine atom in the –CF$_3$ group in (II) is larger than that in the –CH$_3$ group in (I). For reference, the radii of hydrogen and fluorine atoms are 10 and 150 pm, respectively; therefore, the volume of –CF$_3$ is significantly larger than that of –CH$_3$.

Because of this difference between the two substituent atoms, the overall polymer chain structures appeared to be significantly different. Specifically, in the case of hydrogen (I), the main chain is generally linear, whereas in the case of the larger fluorine atom (II), the main chain exhibits a more bent structure. Such structural differences play a crucial role as important variables in explaining future properties.[33]
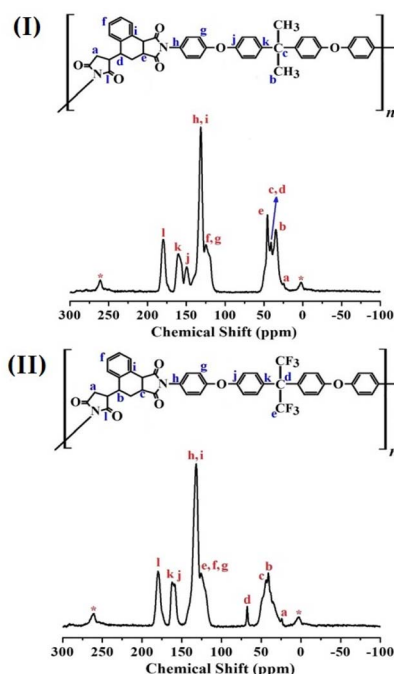
3.3. Solubility

In general, CPI materials must exhibit strong heat and chemical resistance because they are intended for use in flexible displays and electronic applications.[34,35] Because CPIs primarily comprise a benzene structure, melting and chemical dissolution at low temperatures are impractical and pose challenges in processing and recycling. Additionally, mass production *via* roll-to-roll processing is severely limited. The selection of a suitable solvent is crucial for preparing a CPI solution, enhancing its solubility, and improving the film quality during processing. Ultimately, solubility is a pivotal factor for achieving mass production, facilitating easy processing, and promoting recyclability to broaden the application areas of CPI.[36]

Table 2 summarizes the solubility results for the CPIs synthesized using the two diamines. The solubility of the CPI films containing 6FBAPP was significantly better than that of the CPI films containing BAPP. For example, CPI films with
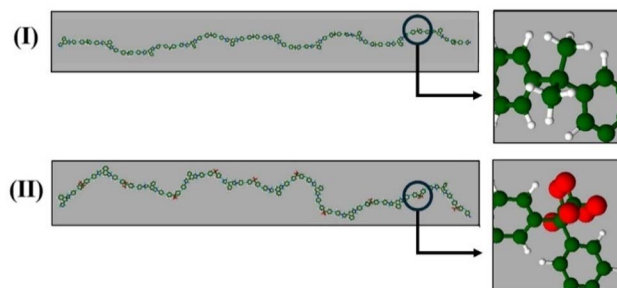

Fig. 3 Comparison of three-dimensional chemical structures of CPIs based on (I) BAPP and (II) 6FBAPP diamine monomers.

Table 2 Solvent tests of CPI films obtained from different monomers[a,b]

Monomer	Act	CHCl₃	CH₂Cl₂	DMAc	DMF	DMSO	Py	THF	EtOH	MtOH	Tol	NMP
BAPP	✕	◎	◎	○	◎	△	○	△	✕	✕	✕	◎
6FBAPP	○	◎	◎	◎	◎	◎	◎	◎	✕	✕	✕	◎

[a] ◎: excellent, ○: good, △: poor, ✕: very poor. [b] Act: acetone, DMAc: *N,N*-dimethylacetamide, DMF: *N,N*-dimethylformamide, DMSO: dimethyl sulfoxide, Py: pyridine, THF: tetrahydrofuran. Tol: toluene, NMP: *N*-methyl-2-pyrrolidone.

BAPP exhibited high solubility in solvents such as chloroform, methylene chloride, *N,N'*-dimethylformamide (DMF), and *N*-methyl-2-pyrrolidone (NMP), but low solubility in general solvents. In contrast, the CPI films containing 6FBAPP demonstrated excellent solubility in all solvents except common solvents like alcohol and toluene. As observed in the already confirmed 3D chemical structure (Fig. 3), these results indicate that the size of the main chain –CF₃ substituent is significantly larger than that of –CH₃, allowing solvents to penetrate easily into the spaces between the bent chains.[37] In conclusion, both synthesized CPI films were nearly insoluble in general solvents but exhibited outstanding solubility in polar solvents.

In general, alicyclic components exhibit significantly higher solubility than benzene. Consequently, various alicyclic structures have recently been incorporated into CPI to enhance the solubility of insoluble PI and improve their processability. The DTDA dianhydride used in this study not only enhanced solubility but also increased optical transparency. The exceptional solubility of our CPIs in various solvents compared to that of many other CPIs was attributed to the utilization of the alicyclic DTDA monomer.

3.4. XRD analysis

XRD was used to investigate the dispersion state and interlayer distance of the clay within the matrix. Although these results were one-dimensional, they allowed the observation of new

crystal forms arising from the dispersion and agglomeration of the clay.

Fig. 4 presents the XRD patterns of the CPI and CPI hybrid films with various organoclay contents. The interlayer distance of pure clay Na⁺-MMT was observed at $2\theta = 7.28°$ ($d = 12.13$ Å); that of organoclay CS30B was observed at $2\theta = 4.98°$ ($d = 17.72$ Å). This indicated that the distance between the clay layers increased because of the substitution of long alkyl groups on the clay surface during the organic modification process. This increased interlayer distance (d) facilitated the insertion of polymer chains during clay dispersion, thereby enhancing dispersibility.[38]

When CS30B was dispersed at 1 wt% in the CPI hybrid films using contents based on (I) BAPP and (II) 6FBAPP diamine monomers the BAPP diamine monomer, no XRD peaks were observed in the hybrid film (see Fig. 4(I)). These results indicate that the clay was well dispersed within the CPI matrix, forming a nanocomposite material. However, when the amount of organoclay reached 2 wt%, peaks were observed at $2\theta = 6.55°$ ($d = 13.48$ Å). These peaks arise from clay agglomeration beyond a certain critical content, which results in the formation of new crystals. The intensity of these peaks increased slightly at the same position as the CS30B content increased to 4 wt%.

In contrast, in Fig. 4(II), using the 6FBAPP diamine monomer, no peak was observed, even when the organoclay was dispersed up to 4 wt%. This implies that the clay was perfectly dispersed in the matrix without agglomeration, thus forming a nanocomposite material. However, these results provide only initial insights into the degree of dispersion; a more detailed morphology must be confirmed using electron microscopy.[39,40]

3.5. Morphology through TEM

While XRD provides information about the interlayer spacing based on the crystallographic structure of the clay, TEM allows direct visualization of the dispersed state of individual clay particles in the hybrid film with much higher resolution. Additionally, TEM can be used to quantitatively observe not only the interlayer orientation of the dispersed clay but also the nanoscale dispersion of the clay within the matrix. In the TEM images presented in this paper, the black hair-like lines represent 1 nm thick clay layers, and the gray spaces between these lines signify gaps between the layers. Specific regions of the clay indicated by arrows are zoomed in and observed in more detail in all photos.

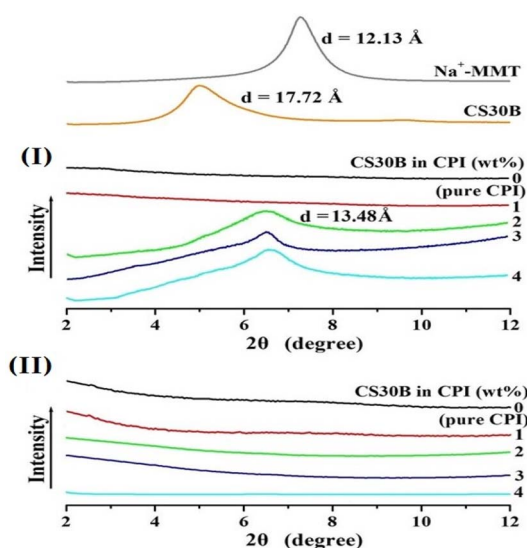Fig. 5 shows TEM images of the hybrid films containing 1 and 2 wt% CS30B in CPI using the BAPP diamine monomer.

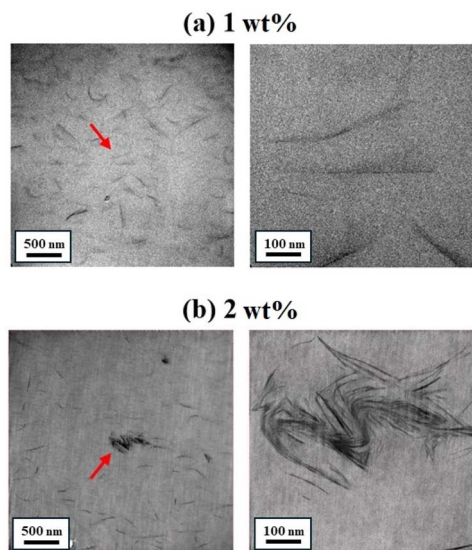**Fig. 4** XRD patterns of CPI hybrid films containing various CS30B.

Fig. 5 TEM images of a CPI hybrid films based on BAPP diamine monomer containing different CS30B contents. (a) 1 wt% and (b) 2 wt%.
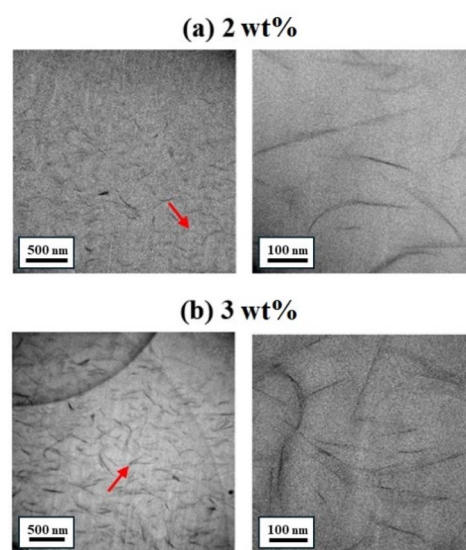

Fig. 6 TEM images of a CPI hybrid films based on 6FBAPP diamine monomer containing different CS30B contents. (a) 2 wt% and (b) 3 wt%.

When the clay content was 1 wt%, the clay exhibited an even dispersion of less than 50 nm (Fig. 5(a)). However, when the clay content was increased to 2 wt%, agglomeration of the clay particles, with sizes reaching ~100 nm, was observed in some areas (Fig. 5(b)). These results indicate that agglomeration occurred when the clay was dispersed above a certain critical content, which confirms the XRD results shown in Fig. 4.

Fig. 6 shows the TEM results of the hybrid films using 2 and 3 wt% CS30B in CPI with the 6FBAPP diamine monomer. When 2 wt% organoclay was employed, very evenly dispersed clay was observed with a thickness of about ≤ 30 nm (Fig. 6(a)). When 3 wt% of organoclay was used, more clay was observed throughout the entire area compared to the 2 wt% hybrid. Although some clay particles measured below 40 nm, most were uniformly dispersed at sizes below 20 nm. As a result, no peaks were observed in the XRD pattern of Fig. 4(II), and as shown in Fig. 6(b), there was no significant difference in the dispersion state compared to the 2 wt% hybrid. In conclusion, it was confirmed that the CPI hybrid synthesized using the two monomers successfully dispersed the clay at the nanoscale. Dispersion at the critical content will have a decisive influence on the thermomechanical properties of the hybrid films described in the future.[41,42]

3.6. Thermal properties

To assess the impact of the differences in the elements contained in the substituents and filler contents on the thermal properties of the hybrids, the thermal properties of the two CPI hybrid series are summarized in Table 3. Generally, because most CPIs are amorphous polymers that lack a crystal structure, a melting transition temperature (T_m) is not observed. Instead, the characteristics of the CPI were elucidated by measuring the glass transition temperature (T_g). T_g is primarily influenced by

the free volume of the substituents and main chain, fluidity of the chain due to segmental motion, main chain rigidity and flexibility, interactions between side chains, and secondary bonds between chains, such as hydrogen bonds.[43,44] Notably, the T_g values of the composite materials mixed with the fillers were significantly influenced by the structure and content of the dispersed fillers.

The T_g values of the hybrid films with various organoclay contents obtained by DSC are listed in Table 3. The T_g value of the CPI hybrid containing BAPP diamine increased from 216 °C for pure CPI to 231 °C when 1 wt% organoclay was dispersed. Even when 6FBAPP was used as a monomer, the T_g of the CPI hybrid with 2 wt% organoclay dispersion was higher (238 °C) than that of pure CPI (227 °C). This increase in T_g can be explained by the thermally highly stable clays that hinder free movement and segmentation of the polymer chains inserted between the clay layers.[45] However, above a certain critical organoclay content, the T_g of the hybrid film decreased. Specifically, when the CS30B content was increased to 4 wt%, the T_g decreased to 221 °C and 230 °C for CPIs containing BAPP and 6FBAPP, respectively (see Table 3). This phenomenon occurred because the clay added to the hybrid film in excess of the critical content was not evenly dispersed and agglomerated, causing a decrease in the thermal properties.[46,47] These results are consistent with the dispersion states observed by XRD and TEM (Fig. 4-6).

When comparing the BAPP and 6FBAPP CPI series, the T_g of the 6FBAPP hybrid is higher than that of the corresponding BAPP hybrid with identical organoclay content. This difference results from the segmental motion of the polymer chain, as the free volume of the –CF$_3$ substituent in the diamine was larger than that of –CH$_3$. In general, when a bulky functional group is substituted in the main chain, the large functional groups hinder the segmental motion of the chain, decrease the chain

Table 3 Thermal properties of PI hybrid films

CS30B in CPI (wt%)	BAPP				6FBAPP			
	T_g (°C)	T_D^{ia} (°C)	wt_R^{600b} (%)	CTE^c (ppm per °C)	T_g (°C)	T_D^i (°C)	wt_R^{600} (%)	CTE (ppm per °C)
0 (pure CPI)	216	404	27	57.7	227	310	19	66.4
1	231	423	40	50.6	233	357	23	53.3
2	228	416	39	48.2	238	389	34	49.8
3	223	410	38	47.0	234	368	33	48.8
4	221	391	37	46.8	230	325	35	48.1

^{a} Initial decomposition temperature at 2% weight loss. ^{b} Weight residue at 600 °C. ^{c} Coefficient of thermal expansion for 2nd heating is 50–200 °C.

mobility, and ultimately increase T_g.[37] Fig. 7 shows the DSC thermograms of CPI hybrids with different CS30B contents.

To investigate the thermal decomposition and stability of the hybrid films, TGA was used to observe their initial decomposition temperature at 2% weight loss (T_D^i) and residual weight amount at 600 °C (wt_R^{600}). The results are summarized in Table 3. T_D^i of the pure CPI containing the BAPP monomer was 404 °C, but when 1 wt% of CS30B was dispersed, the T_D^i increased to 423 °C. Similarly, for pure CPI containing 6FBAPP, the T_D^i was 310 °C, but with a 2 wt% filler content, the T_D^i increased to 389 °C. Uniformly dispersed clay within the CPI matrix improves T_D^i because it acts as a mass-transfer barrier to the volatile products produced by decomposition during heating. Clay is a plate-shaped inorganic material with a very large surface area and a high aspect ratio (length/width, L/W). If the clay particles are evenly dispersed at the nanoscale within the matrix, the mobility of the polymer chains is limited. Additionally, clays with excellent thermal stability, when evenly dispersed within the polymer matrix, delay the polymer-chain decomposition caused by heating and impede free radical diffusion.[48]

However, when the clay was dispersed beyond a certain critical content, the T_D^i of both series decreased. For example, in the CPI hybrid series of BAPP and 6FBAPP, when the organoclay content was increased to 4 wt%, T_D^i decreased to 391 °C and 325 °C, respectively. Regardless of the monomer structure, the phenomenon of T_D^i decreasing above a certain critical content occurred because the excess filler beyond the critical content was not evenly dispersed and therefore agglomerated. As a result, the heat-blocking barrier did not form well, and the polymer chain decomposition was not well suppressed.[49]

The values of wt_R^{600} were highest at the critical clay content but remained almost constant beyond that point. That is, the values of wt_R^{600} hybrids containing BAPP and 6FBAPP increased by 40% and 34%, respectively, at the critical content (Table 3). However, above the critical content, wt_R^{600} remained constant without significant differences. This result is because most polymer materials had already decomposed at a temperature of 600 °C. Fig. 8 shows the TGA thermograms of the CPI hybrids with different CS30B contents.

For a given organoclay content, the thermal stability of the 6FBAPP CPI hybrid series was lower than that of the BAPP hybrid series. This result shows that 6FBAPP, which contains two $-CF_3$ substituents, easily decomposes into fluorine radicals during heating at high temperatures, thereby reducing its thermal stability.[50–52] In addition, the large $-CF_3$ substituent bonded to the main chain causes steric hindrance, making it difficult for the polymer chains to stack in a straight line. The chain packing of 6FBAPP was less efficient than that of BAPP containing the $-CH_3$ group because the bulky fluoride structure distorted the entire chain and caused steric hindrance compared to methyl.[53] For these reasons, the thermal stability of the CPI containing 6FBAPP was lower than that of the CPI containing BAPP.

Polymer materials expand and contract repeatedly as they are heated and cooled. The CTE is a measure of the rate of change in the dimensions of a material according to temperature changes. This is an important consideration for various processes and applications because each polymer material exhibits a unique CTE. Materials with low CTE values exhibit reduced expansion under heat treatment, which can be a positive factor in applications where dimensional stability is important.[54] During the heat treatment, the pure polymer film expanded in a direction perpendicular to the polymer main
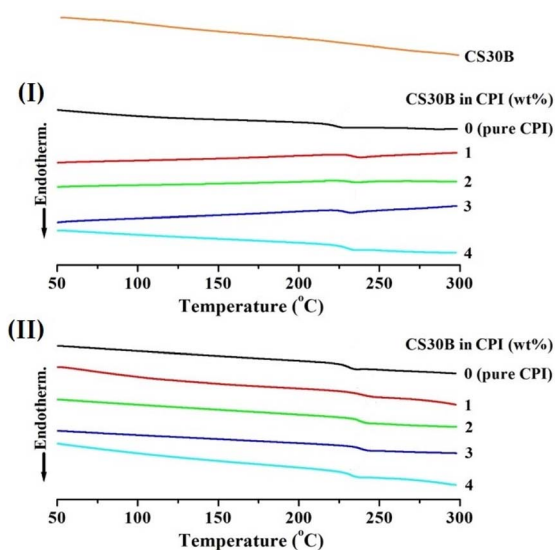

Fig. 7 DSC thermograms of CPI hybrid films containing various CS 30B contents based on (I) BAPP and (II) 6FBAPP diamine monomers.
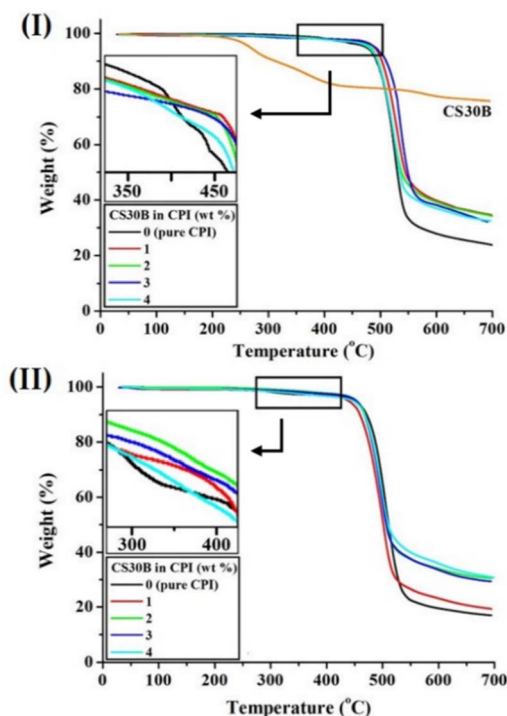
Fig. 8 TGA thermograms of CPI hybrid films containing various CS30B contents based on (I) BAPP and (II) 6FBAPP diamine monomers.

Fig. 9 TMA thermograms of CPI hybrid films containing various CS30B contents based on (I) BAPP and (II) 6FBAPP diamine monomers.

chain. However, a hybrid material with exfoliated plate-like clay layers can exhibit excellent dimensional stability if it does not expand, owing to the high thermal stability and heat barrier properties of the clay.

The TMA results for the two CPI hybrid series with various organoclay contents are shown in Fig. 9 and summarized in Table 3. The CTE decreased with increasing clay content, regardless of the critical content. Specifically, in the BAPP and 6FBAPP hybrid series, as the CS30B content increased from 0 to 4 wt%, the CTE value gradually decreased from 57.7 to 46.8 ppm per °C and from 66.4 to 48.1 ppm per °C, respectively. As previously explained, the CTE decreases with increasing clay content because of the dispersion of hard plate-shaped clay with excellent thermal stability, leading to increased thermal insulation.

When comparing the BAPP and 6FBAPP hybrid series with the same CS30B content in terms of the overall thermal properties, the T_g was higher in the 6FBAPP hybrid series because of the influence of the bulkier –CF_3 substituent. Conversely, the BAPP hybrid series, containing a smaller –CH_3 substituent, had higher $T_D{}^i$, $wt_R{}^{600}$, and CTE values. These results are influenced by the difficulty of segmental movement and the conformation of the overall polymer chain according to the size of the substituents.[55,56]

3.7. Mechanical properties

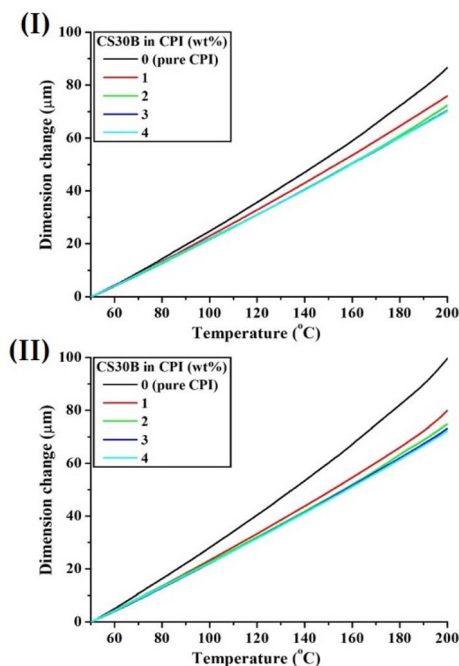The mechanical properties of the CPI hybrids with different monomers were determined by measuring their ultimate strength, initial modulus, and elongation at break (EB). Similar to the thermal properties, the mechanical properties also showed a maximum value at a certain critical content but decreased beyond that point. Table 4 summarizes the mechanical properties of CPI hybrid films with various CS30B contents.

For the BAPP hybrid series, the ultimate tensile strength was 110 MPa in pure CPI and increased to 126 MPa at a 1 wt% of CS30B content. However, the ultimate tensile strength rapidly decreased to 13 MPa at a filler content of 4 wt%. The 6FBAPP series also showed a similar trend, increasing from 91 MPa in pure CPI to 124 MPa at a filler content of 2 wt% and then rapidly decreasing to 11 MPa when the filler content was increased to 4 wt%. The initial modulus also showed the highest value in both the BAPP and 6FBAPP series at the critical clay content but gradually decreased as the clay content increased. For example, in the two hybrid series using BAPP and 6FBAPP monomers, the initial modulus increased to 2.96 and 2.87 GPa at 1 and 2 wt% of CS30B content, respectively, but decreased to 1.24 and 1.19 GPa, respectively, at 4 wt% organoclay content. The mechanical properties according to the dispersed organoclay content are shown in Fig. 10.

The results of the mechanical properties of both series show that they have the highest values at a certain critical organoclay content but decrease significantly beyond the critical content. This can be explained by the aggregation of excess clay above the critical content,[48,49] which has already been confirmed through the dispersion state and aggregation of clay in the XRD and TEM images in Fig. 4–6. The dispersion and orientation of clay within the polymer matrix are closely related to the mechanical properties of the hybrid film. The improvement in

Table 4 Mechanical properties of CPI hybrid films

CS30B in CPI (wt%)	BAPP			6FBAPP		
	Ult. str.[a] (MPa)	Ini. mod.[b] (GPa)	EB[c] (%)	Ult. str. (MPa)	Ini. mod. (GPa)	EB (%)
0 (pure CPI)	110	2.14	5	91	1.60	7
1	126	2.96	5	113	2.64	3
2	55	1.78	4	124	2.87	2
3	34	1.39	2	23	2.04	1
4	13	1.24	1	11	1.19	1

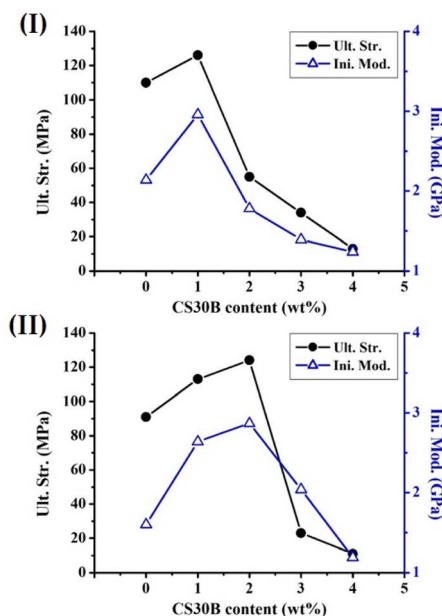[a] Ultimate strength. [b] Initial modulus. [c] Elongation at brea.

Fig. 10 Mechanical properties of CPI hybrid films containing various CS30B contents based on (I) BAPP and (II) 6FBAPP diamine monomers.

excess clay was not evenly distributed and existed in clumps, which eventually led to lower light transmission and a darker color. PI appears dark brown because its main-chain π electrons absorb purple and blue-green colors within the visible light range of 400 to 500 nm while reflecting contrasting yellow and red colors.[58]

The optical transparency of the CPI hybrid film was evaluated considering λ_0, which represents the initial transmission wavelength, the transmittance at 500 nm (500 nm[trans]) in the visible light region, and the YI. Fig. 11 shows the transmittance of the CPI hybrid film according to the CS30B content obtained using UV-Vis spectroscopy; the results are summarized in Table 5. Although there was no significant difference, as the content of organic clay increased from 0 to 4 wt% for both the BAPP and
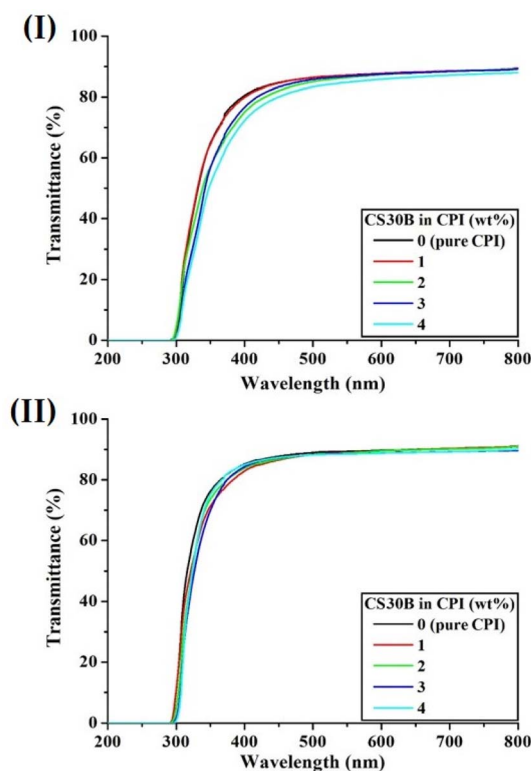
the mechanical properties is influenced by the high-strength clay itself, which is uniformly distributed at the nanoscale, but can also be explained by the excellent orientation of the dispersed clay in the matrix.

As the organoclay content increased from 0 to 4 wt% in the BAPP and 6FBAPP hybrid series, the EB values decreased from 5% to 1% and from 7% to 1%, respectively. These results exemplify the typical case of a hybrid material in which a composite reinforced with an inorganic material, such as clay, is hard but brittle.[57]

3.8. Optical transparency

There is a significant relationship between the dispersed clay content of the hybrid films and their optical properties. In a hybrid film in which plate-shaped clay was exfoliated and isotropically dispersed within the matrix, the light transmittance was excellent, and the transparency of the hybrid film was maintained. However, as the clay content increased, the

Fig. 11 UV-vis transmittance (%) of CPI hybrid films containing various CS30B contents based on (I) BAPP and (II) 6FBAPP diamine monomers.

Table 5 Optical properties of CPI hybrid films

CS30B in CPI (wt%)	BAPP				6FBAPP			
	Thickness[a] (μm)	λ_0[b] (nm)	500 nm[trans] (%)	YI[c]	Thickness (μm)	λ_0 (nm)	500 nm[trans] (%)	YI
0 (pure PI)	44	292	88	<1	43	291	89	<1
1	45	294	86	1	45	291	88	1
2	44	294	85	1	45	293	88	1
3	45	297	85	2	46	296	88	1
4	45	297	83	3	44	297	88	2

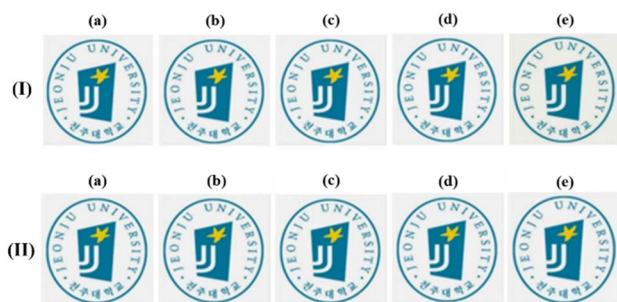[a] Film thickness. [b] Cut off wavelength. [c] Yellow index.

Fig. 12 Photographs of CPI hybrid films containing various CS30B contents based on (I) BAPP and (II) 6FBAPP. (a) 0 (pure CPI), (b) 1, (c) 2, (d) 3, and (e) 4 wt% CS30B.

6FBAPP series, the λ_0 value also increased from 292 to 297 nm and 291 to 297 nm, respectively. This indicates that all hybrid films, irrespective of their monomer and filler contents, begin initial transmission before reaching the visible light region. The 500 nm[trans] of the hybrid series containing two monomers slightly decreased with increasing clay content but remained above 80% for all hybrid films (Table 5). Based on the results of λ_0 and 500 nm[trans], it was found that the transparency of all hybrid films was excellent regardless of monomer type and filler content.

Clay is a multilayered mineral with a thickness of 1 nm. In the hybrid films, as the dispersed clay content increased, the light transmittance decreased because of clay aggregation. However, when clay is exfoliated at the nanometer scale, optically colorless and transparent films with very low YI values can be obtained. Pure CPI synthesized using two different monomers exhibited YI values below 1, appearing colorless and transparent, like glass. Even when the clay content was increased to 4 wt%, the hybrid films of both series exhibited YI values of 2–3. From these YI values, it can be inferred that the hybrid films demonstrated optical properties comparable to those of films that could replace glass.

To assess visual optical transparency, pure CPI and CPI hybrid films were placed on a university logo and photographed. The results are compared in Fig. 12. When the organoclay content was 4 wt%, slightly inferior optical properties were observed compared to 0–3 wt%. However, when the logo was visually observed on the film, almost no noticeable

difference was observed. Overall, there was no significant difference in the optical transparency. However, the transparency of the CPI hybrid film containing 6FBAPP was slightly higher than that of the CPI hybrid film containing the BAPP monomer. This is attributed to the strongly electron-withdrawing CF$_3$ group, which suppresses the CTC effect.[37,59]

4. Conclusions

In this study, we designed a new CPI structure using different diamine monomers and investigated the effects of dispersing various amounts of organic nanofillers on the properties of CPI hybrid films. Hybrid films were produced using MMT-based organoclay CS30B at concentrations ranging from 1 to 4 wt% relative to CPI. We examined the solubility, thermomechanical properties, dispersed clay morphology, and optical properties and compared the results.

The T_g of the 6FBAPP hybrid film, which contained a large substituent (–CF$_3$), was higher than that of the hybrid film containing BAPP, regardless of the clay content. However, the T_D[i], wt$_R$[600], and CTE values of the CPI hybrid using the BAPP monomer, which contains a small substituent (–CH$_3$), were superior to those of the CPI containing 6FBAPP because of its linear polymer chain structure and low steric hindrance. For the same reason as steric hindrance, the mechanical properties of the BAPP hybrid were better than those of the 6FBAPP hybrid at the same organoclay content. Although the difference was not significant, the optical transparency of the CPI hybrid containing the 6FBAPP monomer was superior to that of the BAPP hybrid because it contained a strongly electron-withdrawing CF$_3$ group that interfered with the CTC. In particular, an optical transparency comparable to that of general-purpose glass was observed in the CPI hybrid film with low organoclay content.

Fluorine is a highly reactive element; although it can exhibit long-term stability in the environment, increasing concentrations can pose risks to ecosystems and human health. Therefore, it is important to manage fluorine emissions and continuously monitor its levels in the environment. For a long time, various monomers containing environmentally harmful fluorine have been used to synthesize CPI, and the synthesized CPI films have very low solubility, making environmentally friendly post-processing difficult. However, based on the results

of this study, it is now recognized that CPI with halogen-free monomer structures can also be excellent alternative materials with useful physical properties. When electronic and electrical materials require high heat resistance and insulation, CPI hybrids with such capabilities can be used. They can also be used in display circuit boards because of their thinness, flexibility, and transparency. Moreover, they can be applied in fields requiring more stringent processes and higher performances.

Data availability

The datasets used and/or analysed during the current study are available from the corresponding author on reasonable request.

Author contributions

J.-H. Chang designed the study and drafted the manuscript. A. R. Lim analyzed NMR and X-ray experiments. M. Y. Choi prepared the samples and participated in data analysis. All the authors have read and agreed to the published version of the manuscript.

Conflicts of interest

The authors declare no conflict of interest.

References

1 C. Yi, W. Li, S. Shi, K. He, M. Chen and C. Yang, *Sol. Energy*, 2020, **195**, 340–354.
2 R. J. Iredale, C. Ward and I. Hamerton, *Prog. Polym. Sci.*, 2017, **69**, 1–21.
3 T. Xiao, X. Fan, D. Fan and Q. Li, *Polym. Bull.*, 2017, **74**, 4561–4575.
4 H. Gao, X. Lan, L. Liu, X. Xiao, Y. Liu and J. Leng, *Smart Mater. Struct.*, 2017, **26**, 095001.
5 I. Gouzman, E. Grossman, R. Verker, N. Atar, A. Bolker and N. Eliaz, *Adv. Mater.*, 2019, **31**, 1807738.
6 J. Kim, S. Shrestha, M. Souri, J. G. Connell, S. Park and A. Seo, *Sci. Rep.*, 2020, **10**, 12486.
7 M. R. Azani, A. Hassanpour and T. Torres, *Adv. Energy Mater.*, 2020, **10**, 220536.
8 Y. Y. Liu, J.-H. Cao, Y. Wang, S.-G. Shen, W.-H. Liang and D.-Y. Wu, *ACS Appl. Polym. Mater.*, 2022, **4**, 7664–7673.
9 R.-D. Rusu, C.-P. Constantin, M. Drobota, L.-M. Gradinaru, M. Butnaru and M. Pislaru, *Polym. Degrad. Stab.*, 2020, **177**, 109182.
10 L. Zhou, D. Shen, P. Gou, L. He, F. Xie, C. He, G. Hu and R. Chen, *Chem. Eng. J.*, 2023, **477**, 146992.
11 M. Zhang, J. Miao, Y. Xu, Z. Wang and J. Yan, *Macromolecules*, 2022, **55**, 7992–8001.
12 Z. Wang, Z. He, X. Ren, Y. Zhang, X. Wang, C. Yang, S. Han, H. Yu and J. Liu, *J. Appl. Polym. Sci.*, 2024, e55606.
13 X. Ren, H. Wang, X. Du, H. Qi, Z. Pan, X. Wang, S. Dai, C. Yang and J. Liu, *Materials*, 2022, **15**, 6346.
14 S. Yu, J. Zhou, A. Xu, J. Lao, H. Luo and S. Chen, *Chem. Eng. J.*, 2023, **469**, 143803.
15 L. Wu, H. Wang, Y. An, Y. Jia, Y. Tan, X. Wei, X. Zhi, Y. Zhang and J. Liu, *J. Polym. Res.*, 2021, **28**, 310.
16 X. Zhi, H. Wang, X. Wei, Y. Zhang, Y. An, J. Qi and J. Liu, *Nanomaterials*, 2021, **11**, 1977.
17 Y. Zhang, W. H. Lee, J. G. Seong, J. Y. Bae, Y. Zhuang, S. Feng, Y. Wan and Y. M. Lee, *J. Membr. Sci.*, 2020, **611**, 118363.
18 A. I. Barzic, R. M. Albu, I. Stoica, C. D. Varganici and C. Hulubei, *Polym. Bull.*, 2023, **80**, 4503–4522.
19 T. Matsumoto, *Macromolecules*, 1999, **32**, 4933–4939.
20 T. Matsumoto and J. Synth, *Org. Chem. Jpn.*, 2000, **58**, 776–786.
21 V. E. Ogbonna, P. Popoola, O. M. Popoola and S. O. Adeosun, *J. Thermoplast. Compos. Mater.*, 2021, **36**, 1–30.
22 D. Ai, H. Li, Y. Zhou, L. Ren, Z. Han, B. Yao, W. Zhou, L. Zhao, J. Xu and Q. Wang, *Adv. Energy Mater.*, 2020, **10**, 1903881.
23 S. Xing, Z. Pan, X. Wu, H. Chen, X. Lv, P. Li, J. Liu and J. Zhai, *J. Mater. Chem. C*, 2020, **8**, 12607–12614.
24 M. H. Nazari, Y. Zhang, A. Mahmoodi, G. Xu, J. Yu, J. Wu and X. Shi, *Prog. Org. Coat.*, 2022, **162**, 106573.
25 A. D. de Oliveira and C. A. G. Beatrice, *Nanocomposites*, 2018, **6**, 103–128.
26 M. Y. Choi, S. J. Lee, A. R Lim and J.-H. Chang, *Sci. Rep.*, 2022, **12**, 20892.
27 S. J. Lee, M. Y. Choi, L. K. Kwac, H. G. Kim and J.-H. Chang, *Rev. Adv. Mater. Sci.*, 2023, **62**, 20230120.
28 E. J. Baileym and K. I. Winey, *Prog. Mater. Sci.*, 2020, **105**, 101242.
29 H. H. Murray, *Appl. Clay Sci.*, 1991, **5**, 379–395.
30 Y. Yang, Z.-K. Zhu, J. Yin, X.-Y. Wang and Z.-E. Qi, *Polymer*, 1999, **40**, 4407–4414.
31 D. L. Pavia, G. M. Lampman, G. S. Kriz and J. R. Vyvyan, *Introduction to Spectroscopy*, Cengage Learning, Boston, Massachusetts, USA, 2008, Ch. 2, p. 14.
32 D. L. Pavia, G. M. Lampman, G. S. Kriz and J. R. Vyvyan, *Introduction to Spectroscopy*, Cengage Learning, Boston, Massachusetts, USA, 2008, Ch. 4, p. 146.
33 S. S. Ray and M. Okamoto, *Prog. Polym. Sci.*, 2003, **28**, 1539–1641.
34 P. Ma, C. Dai, H. Wang, Z. Li, H. Liu, W. Li and C. Yang, *Compos. Commun.*, 2019, **16**, 84–93.
35 Z. Yang, P. Ma, F. Li, H. Guo, C. Kang and L. Gao, *Eur. Polym. J.*, 2021, **148**, 110369.
36 A. Chandrasekaran, C. Kim, S. Venkatram and R. Ramprasad, *Macromolecules*, 2020, **53**, 4764–4769.
37 A. X. Wu, J. A. Drayton, K. M. Rodriguez, Q. Qian, S. Lin and Z. P. Smith, *Macromolecules*, 2020, **53**, 5085–5095.
38 R. A. Vaia and E. P. Giannelis, *Macromolecules*, 1997, **30**, 8000–8009.
39 A. B. Morgan and J. W. Gilman, *J. Appl. Polym. Sci.*, 2003, **87**, 1329–1338.
40 J. Ma, J. Xu, J.-H. Ren, Z.-Z. Yu and Y.-W. Mai, *Polymer*, 2003, **44**, 4619–4624.
41 C. Akinyi and J. O. Iroh, *Polymers*, 2023, **15**, 299.
42 P. Ma, C. Dai, H. Wang, Z. Li, H. Liu, W. Li and C. Yang, *Compos. Commun.*, 2019, **16**, 84–93.

43 G. Zhu, H. Lao, F. Feng, M. Wang, X. Fang and G. Chen, *Eur. Polym. J.*, 2022, **179**, 111558.

44 L. Jiao, F. Luo, Z. Du, X. Dai, J. Mu, H. Wang, Z. Dong and X. Qiu, *React. Funct. Polym.*, 2022, **181**, 105449.

45 X. Ma, F. Zheng, C. G. C. E. van Sittert and Q. Lu, *J. Phys. Chem. B*, 2019, **123**, 8569–8579.

46 S. Esmaielzadeh and H. Ahmadizadegan, *J. Thermoplast. Compos. Mater.*, 2024, **37**, 363–386.

47 H. Baniasadi, J. Trifol, A. Ranta and J. Seppälä, *Composites, Part B*, 2021, **211**, 108655.

48 U. Min, J.-C. Kim and J.-H. Chang, *Polym. Eng. Sci.*, 2011, **51**, 2143–2150.

49 Y. Na, L. K. Kwac, H. G. Kim, Y. L. Joo and J.-H. Chang, *RSC Adv.*, 2023, **13**, 16285–16292.

50 H. Jeon, L. K. Kwac, H. G. Kim and J.-H. Chang, *Rev. Adv. Mater. Sci.*, 2022, **61**, 394–404.

51 P. Politzer and J. S. Murray, *J. Mol. Model.*, 2019, **25**, 1–12.

52 W. R. Dolbier, *Chem. Rev.*, 1996, **96**, 1557–1584.

53 E. Giannetti, *J. Fluorine Chem.*, 2005, **126**, 623–630.

54 M. Hasegawa, *Polymers*, 2017, **9**, 520.

55 R. Kunz, T. Martin, C. Callsen, J. Hutschreuther, V. Altstädt and J. Breu, *Polymer*, 2019, **169**, 74–79.

56 J. Y. Park and D. R. Paul, *J. Membr. Sci.*, 1997, **125**, 23–39.

57 H. I. Shin and J.-H. Chang, *Polymers*, 2020, **12**, 135.

58 C.-P. Yang, S.-H. Hsiao and Y.-C. Chen, *J. Appl. Polym. Sci.*, 2005, **97**, 1352–1360.

59 S. A. Holmes and T. D. Thomas, *J. Am. Chem. Soc.*, 1975, **97**, 2337–2341.